

MULTIDISCIPLINARY DESIGN OPTIMIZATION OF A THREE-DIMENSIONAL SUPERSONIC BIPLANE BASED ON METHOD OF CHARACTERISTICS

Yuki UTSUMI

Institute of Fluid Science, Tohoku University, Sendai 980-8577, JAPAN

Keywords: *Supersonic flow, Multidisciplinary optimization, Method of Characteristics*

Abstract

This paper discusses a multidisciplinary design optimization of a three-dimensional supersonic biplane. First, methods to evaluate the performance of a supersonic biplane are described. The methods include modified oblique shock wave equations, a modified Method of Characteristics, and the reference enthalpy method. Second, validations of the present methods are described. Finally, a multidisciplinary design optimization was conducted in terms of aerodynamic performance and weight performance, and trade-off relationship between them is shown. Major factors governing the trade-off relationship are found out and characteristics of a supersonic biplane are described.

1 Introduction

A bottleneck in the development of commercial supersonic transport aircrafts is a strong sonic boom felt on the ground. A strong sonic boom has been preventing supersonic aircrafts from flying over the land. It restricts the flexibility of operations and thus makes the value of supersonic aircrafts low. Hence, supersonic aircrafts need to be so designed as to meet requirements on a sonic boom.

Busemann [1] mentioned that the two-dimensional biplane shown in Fig. 1 does not generate drag in an inviscid supersonic flow by the interferences of the shock and the expansion waves. Later, Lomax [2] confirmed in a linearized flow that the equivalent source strength of such biplane is zero throughout although the biplane has a finite thickness. It means that the biplane can eliminate the

contribution of wing volume to the pressure disturbance on the ground or a sonic boom. Hence, the biplane is a useful concept for supersonic aircraft design under constraints on sonic booms because the pressure disturbance due to wing volume can be compensated for by the contributions of other aircraft components to a sonic boom [3].

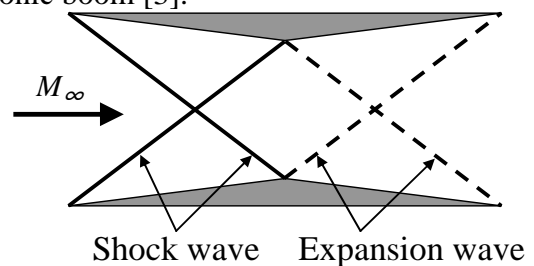


Fig. 1 Supersonic Biplane Concept

There have been researches aiming at designing a three-dimensional supersonic biplane with high aerodynamic performance [4-7]. Maruyama et al. [5,6] conducted it by employing an inverse design method. This method found a wing shape of which the surface pressure distribution matches a user-specified target one. However, this method has two limitations. First, it is difficult to come up with target pressure distribution that yields high aerodynamic performance. Second, it only take into account pressure force although other characteristics, e.g. friction force, wing weight, etc., are also important.

The present study conducted multidisciplinary optimization of a three-dimensional supersonic biplane to overcome the limitations of the previous research. Optimization objectives were to maximize aerodynamic performance including viscous effect and to minimize the wing weight. Because no detailed configuration of a

supersonic aircraft with the biplane has been presented so far, many uncertainties in design requirements would exist. Thus, a computationally inexpensive design process is desirable to make it possible to redesign the biplane quickly when the requirements change. This study employed modified oblique shock wave equations, a modified Method of Characteristics (MOC), the reference enthalpy method to promptly evaluate the aerodynamic performance of the biplane, and an analytical method to evaluate the wing weight. These methods were incorporated with the genetic algorithm (GA) to obtain optimal shapes of supersonic biplanes in terms of the aerodynamics and the wing weight.

2 Development of Analysis Tool

2.1 Geometry Definition

A supersonic biplane in the present study is a tapered and swept wing without twist. It has the airfoil similar at any spanwise stations, and has a planar shape defined by straight lines. The three-dimensional shape of a supersonic biplane is defined by the sweep and the dihedral angle of the lower wing leading edge, the taper ratio, and the ratio of span length to the vertical gap between the upper and the lower wing at the leading edges.

An airfoil geometry definition basically follows the Licher's definition [8] with some modifications to allow greater flexibility of geometry. An airfoil shape is defined by seven design variables and two fourth-order polynomials that smoothly start from the point at which the expansion fan first hits the other wing as shown in Fig. 2. The reason why the aft parts of the inward surfaces are defined by the polynomials is due to spread of an expansion fan. A supersonic biplane was introduced within the assumption that the airfoil is infinitely thin and expansion waves are expressed by line. However, an expansion wave spreads out to be an expansion fan in general, and thus the pressure distribution on the inward aft surface deviates from the ideal one that results in zero wave drag [1]. Hence, the aft surface of the

airfoil is defined by a high-order flexible curve to yield low drag.

Once these design variables are given, an airfoil is constructed so that the shock wave from each wing leading edge hits the inward vertex of the other wing using modified oblique shock equations that will be introduced in the next section.

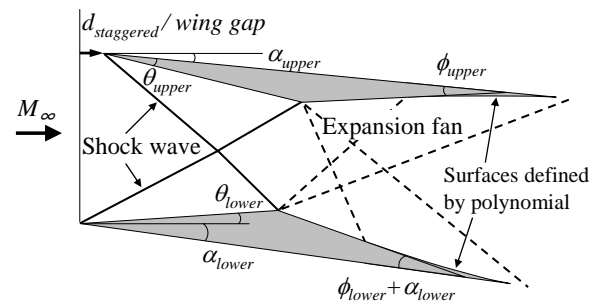


Fig. 2 Airfoil Geometry Definition

2.2 Evaluation Methods

2.2.1 Pressure force evaluation

To evaluate pressure force, the three-dimensional steady Euler equations are considered as governing equations. To solve them, the oblique shock wave equations and MOC are employed. Generally, these methods cannot be applied to a three-dimensional flow [9]. The oblique shock wave equations can be applied to shock waves perpendicular to a plane in consideration. Three-dimensional shock waves in general do not satisfy this condition. MOC is based on the equations given by diagonalizing Euler equations, but such a diagonalization is impossible in three dimensions.

The present study proposes a method to apply those methods to the three-dimensional flow field around a supersonic biplane defined by the previous section. For the supersonic biplane in the present study, flow field around the biplane that is outside of the Mach cones from the wing tips and wing roots can be locally considered as two-dimensional by local coordinate transformation. This coordinate transformation is carried out such that the derivative with respect to a third coordinate is zero or negligible. Such a coordinate transformation is impossible inside the Mach cones from the wing tips and wing roots. Thus,

the employed methods cannot be used inside such regions accurately. In the present study, a region in which the local coordinate transformation is possible is called an ideal region, whereas the other region is called an unideal region.

After the coordinate transformation, the oblique shock wave equations can be applied to the flow field. Hence, shock waves in the ideal region can now be solved.

Next, a method to apply MOC is described herein. The three-dimensional steady Euler equations are given by Eq. (1).

$$\frac{\partial E}{\partial x} + \frac{\partial F}{\partial y} + \frac{\partial G}{\partial z} = 0 \quad (1)$$

where

$$E = \begin{bmatrix} \rho u \\ p + \rho u^2 \\ \rho uv \\ \rho uw \\ \rho uH \end{bmatrix}, F = \begin{bmatrix} \rho v \\ \rho vu \\ p + \rho v^2 \\ \rho vw \\ \rho vH \end{bmatrix}, G = \begin{bmatrix} \rho w \\ \rho wu \\ \rho wv \\ p + \rho w^2 \\ \rho wH \end{bmatrix} \quad (2)$$

ρ is the density, p is the pressure, u , v , and w are the velocity components in x , y , and z directions, respectively, and H is a specific total enthalpy. Choosing the coordinate system in which the derivative with respect to y is zero yields Eq. (3).

$$\frac{\partial E}{\partial x} + \frac{\partial G}{\partial z} = 0 \quad (3)$$

that are

$$\text{Continuity: } \frac{\partial \rho u}{\partial x} + \frac{\partial \rho w}{\partial z} = 0 \quad (4)$$

$$\text{x-momentum: } \frac{1}{\rho} \frac{\partial p}{\partial x} + u \frac{\partial u}{\partial x} + w \frac{\partial u}{\partial z} = 0 \quad (5)$$

$$\text{y-momentum: } u \frac{\partial v}{\partial x} + w \frac{\partial v}{\partial z} = 0 \quad (6)$$

$$\text{z-momentum: } u \frac{\partial w}{\partial x} + w \frac{\partial w}{\partial z} + \frac{1}{\rho} \frac{\partial p}{\partial z} = 0 \quad (7)$$

$$\text{Energy: } u \frac{\partial H}{\partial x} + w \frac{\partial H}{\partial z} = 0 \quad (8)$$

Equations (6) and (8) yield

$$u \frac{\partial H'}{\partial x} + w \frac{\partial H'}{\partial z} = 0 \quad (9)$$

where $H' = H - v^2/2$. Equations (4), (5), (7), and (9) are the same as the two-dimensional Euler equations. Hence, those equations can be diagonalized to yield Eq. (10).

$$\frac{\partial V_i}{\partial t} + \lambda_i \frac{\partial V_i}{\partial n} = 0 \quad (10)$$

where

$$dV_1 = \frac{\sqrt{M'^2-1}}{q'} dq' + d\varphi' + \frac{1}{\gamma(\gamma-1)} \frac{\sqrt{M'^2-1}}{M'^2} d\bar{s} - \frac{\sqrt{M'^2-1}}{q'^2} dH' \quad (11)$$

$$dV_2 = d\bar{s} \quad (12)$$

$$dV_3 = dH' \quad (13)$$

$$dV_4 = -\frac{\sqrt{M'^2-1}}{q'} dq' + d\varphi' - \frac{1}{\gamma(\gamma-1)} \frac{\sqrt{M'^2-1}}{M'^2} d\bar{s} + \frac{\sqrt{M'^2-1}}{q'^2} dH' \quad (14)$$

$$\lambda_1 = -\tan \mu' \quad (15)$$

$$\lambda_2 = 0 \quad (16)$$

$$\lambda_3 = 0 \quad (17)$$

$$\lambda_4 = \tan \mu' \quad (18)$$

M is the Mach number, q is the velocity, φ is the angle between in-plane velocity vector and t coordinate, γ is the specific heat ratio, $\bar{s} = s/c_v$, s is the entropy, c_v is the specific heat at constant volume, and $\mu = \arcsin(1/M)$. t indicates the coordinate along in-plane velocity vector and n indicates the in-plane coordinate perpendicular to t . The variables with a prime are calculated using only in-plane variables. Equations (10)-(18) indicate that $dV_i = 0$ along a line with $(dn/dt) = \lambda_i$.

Consider a net constructed by characteristics shown in Figure 3. Actual characteristics are shown by blue whereas red lines are employed as characteristics in the

present method. The red lines are straight with their gradients being the gradients of the characteristics at points A and B , respectively. Two sets of lines are different but almost the same if the points A and B are close.

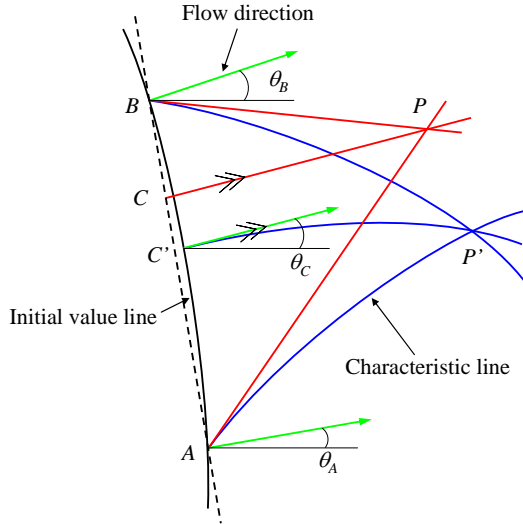


Fig. 3 Net constructed by characteristic lines

If a shock wave is absent, the entropy is constant. Hence, the third term in Eqs. (11) and (14) vanishes. Because of the coordinate transformation, in-plane specific total enthalpy is not constant throughout the flow field. Assume the point P is close enough to the points A and B for the variables on the characteristics $B-P$ and $A-P$ to be assumed constant. On this assumption, the Eqs. (11), (13), and (14) are integrated to yield

$$\begin{aligned} v'_B + \phi'_B - \frac{\sqrt{M_B'^2 - 1}}{M_B'^2 \gamma R T_B} H'_B \\ = v'_P + \phi'_P - \frac{\sqrt{M_B'^2 - 1}}{M_B'^2 \gamma R T_B} H'_P \end{aligned} \quad (19)$$

$$\begin{aligned} -v'_A + \phi'_A + \frac{\sqrt{M_A'^2 - 1}}{M_A'^2 \gamma R T_A} H'_A \\ = -v'_P + \phi'_P + \frac{\sqrt{M_A'^2 - 1}}{M_A'^2 \gamma R T_A} H'_P \end{aligned} \quad (20)$$

$$H'_P = H'_C \quad (21)$$

where ν is the Prandtl–Meyer function, T is the temperature, and R is the specific gas constant.

Variables at the point C are linearly interpolated using the variables at the point A and B . Flow field without any discontinuities can be obtained by simultaneously solving the Eqs. (19)-(21).

Except shock waves, there is a discontinuity shown in Fig. (4) in the flow field around the supersonic biplane across which the entropy is discontinuous. Special treatment to be proposed below is needed to solve this discontinuity.

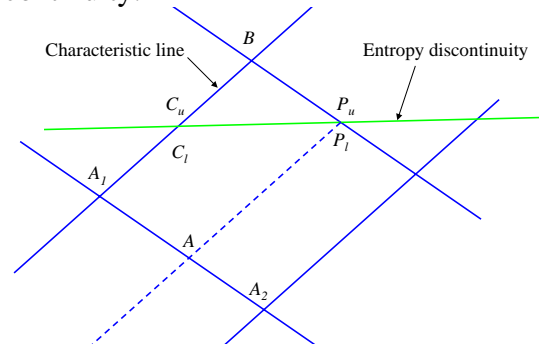


Fig. 4 Net constructed by characteristic lines across entropy discontinuity

From the first law of thermodynamics,

$$Tds = c_v dT + pd\left(\frac{1}{\rho}\right) \quad (22)$$

The specific total enthalpy is constant throughout flow field and the pressure does not change across the entropy discontinuity. Using these conditions and Eq. (22) give

$$ds = -\frac{\gamma R}{1 + \frac{\gamma - 1}{2} M^2} M dM \quad (23)$$

This can be integrated to yield

$$M = \sqrt{\frac{C \exp\left(-\frac{\gamma - 1}{\gamma R} s\right) - 2}{\gamma - 1}} \quad (24)$$

$$\text{where } C = \frac{2 + M_o^2(\gamma - 1)}{\exp\left(-\frac{\gamma - 1}{\gamma R} s_o\right)} \quad (25)$$

Subscript o indicates a value on the opposite side of the entropy discontinuity. Equations (11) and (14) with the Eqs. (23), the equation of state, and $dp=0$ across the entropy discontinuity become

$$dV^\mp = d\phi \quad (26)$$

With Eq. (10), Eq. (26) means that flow angle does not change across the entropy discontinuity.

Consider the point P_u in Fig. 4. The Mach number is decomposed into in-plane component M'_{Pu} and out-of-plane component M_{Puy} :

$$M_{Pu}^2 = M'^2_{Pu} + M^2_{Puy} \quad (27)$$

The out-of-plane Mach number component is given by

$$M^2_{Puy} = \frac{2}{\gamma RT_{Pu}} (H_\infty - H'_{Pu}) \quad (28)$$

Equations (27), (28) and the isentropic equation yield

$$M_{Pu} = \sqrt{\frac{M'^2_{Pu} \gamma RT_B \left(1 + \frac{\gamma-1}{2} M_B^2\right) + 2(H_\infty - H'_{Pu})}{\gamma RT_B \left(1 + \frac{\gamma-1}{2} M_B^2\right) - (H_\infty - H'_{Pu})(\gamma-1)}} \quad (29)$$

Similarly for the point P_l there exists a relationship

$$M_{Pl} = \sqrt{\frac{M'^2_{Pl} \gamma RT_A \left(1 + \frac{\gamma-1}{2} M_A^2\right) + 2(H_\infty - H'_{Pl})}{\gamma RT_A \left(1 + \frac{\gamma-1}{2} M_A^2\right) - (H_\infty - H'_{Pl})(\gamma-1)}} \quad (30)$$

The variables at the point A is linearly interpolated from the variables at A_1 and A_2 . By simultaneously solving Eqs. (19)-(21), (24), (25), (29), and (30) the variables at the points P_u and P_l are obtained. With the equations given so far, the three-dimensional Euler equations are solved in the ideal region.

2.2.2 Friction force evaluation

The Euler equations have been employed as governing equations of flow field. The Euler equations neglect viscous effect, that is, friction force. Hence, the friction force needs to be evaluated separately.

The reference enthalpy method [10] was employed to evaluate friction force. This method estimates the friction drag of a compressible flat plate boundary layer by applying reference enthalpy into the estimation equation for incompressible boundary layer.

The friction force of the biplane was approximated by two flat plates and fully turbulent boundary layer was assumed in this method.

From the reference enthalpy, the reference temperature can be calculated by

$$\frac{T^*}{T_e} = 0.5 \left(1 + \frac{T_w}{T_e}\right) + 0.16r \left(\frac{\gamma-1}{2}\right) M_e^2 \quad (31)$$

where T^* is the reference temperature, T_e is the temperature at outer edge of the boundary layer, M_e is the Mach number at outer edge of the boundary layer, r is the recovery factor, e denotes a value at outer edge of boundary layer, w denotes a value at wall,

$$\frac{T_w}{T_e} = 1 + r \left(\frac{T_0}{T_e} - 1\right) \quad (32)$$

and 0 denotes the value of the total condition. The recovery factor for turbulent flow is approximately given by $r = Pr^{1/3}$ where Pr is the Prandtl number. With the reference temperature, the reference density is given by state equation and the reference viscosity coefficient by Sutherland viscosity law. The approximation equation for estimating skin friction coefficient of incompressible flat plate turbulent boundary layer is

$$c_f = \frac{0.02296}{Re_x^{0.139}} \quad (33)$$

where Re_x is the Reynolds number based on local distance from a leading edge. Replacing the Reynolds number in Eq. (33) by the one given by the reference density and the reference viscosity coefficient yields the skin friction coefficient of a compressible flat plate turbulent boundary layer.

$$c_f = \frac{0.02296}{Re_x^{0.139}} \left(\frac{\rho^*}{\rho_e}\right)^{0.861} \left(\frac{\mu^*}{\mu_e}\right)^{0.139} \quad (34)$$

where μ is the viscosity coefficient, and the asterisk indicates reference value.

2.2.3 Weight estimation

The analytical method [11] has been employed to evaluate wing weight. This method calculates a required weight of a wing structure based on the bending moment obtained by aerodynamic

analysis. This value and the wing area yield an estimation of wing weight based on the correlation data of existing aircrafts.

Consider a cross-sectional structure of the lower wing shown in Fig. 5. The red lines show structures that carry loads. The front and aft parts are not used to carry loads because these parts are necessary for moving parts to avoid choking of the wing [4].

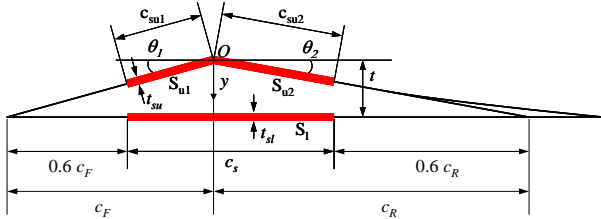


Fig. 5 Wing structure for weight estimation

Maximum bending moment of the wing is calculated from aerodynamic force. Aircrafts have to withstand loads under the ultimate load factor condition. The ultimate load factor is 1.5 times the limit load factor which, by FAA Federal Aviation Regulations, is given by $2.1+24000/(W_0+10000)$ where W_0 is the design maximum takeoff weight. A previous study showed that sum of forces acting on inward surfaces of a supersonic biplane does not almost change when the angle of attack is changed [12]. Thus, pressure force acting on each wing in the ultimate load factor condition is calculated only by changing the outward surface pressure.

Bending moment M_b and normal stress σ has a relationship:

$$\sigma = \frac{M_b t/2}{I_G} \quad (35)$$

where I_G is a second moment of cross sectional area of structure. The second moment of cross sectional area is related to the cross sectional area A . Maximum stress of the wing material is given. Substitution of maximum bending moment to Eq. (35) gives required cross sectional area of wing structure which yields the minimum weight of wing box $W_{wingbox}$.

$$W_{wingbox} = \rho_{mat} g \int Adl = \frac{\rho_{mat} g}{\cos \Omega' \cos \tau} \int_0^{b/2} Ady \quad (36)$$

where ρ_{mat} is the density of material, g is the acceleration due to gravity, l is the coordinate

along the structural axis, Ω' is the sweep angle, τ is the dihedral angle, and b is the wing span. The minimum weight of a wing box and the wing area S have a statistical relationship with overall wing weight given by

$$W_{wing} = 1.30W_{wingbox} + 29.44S \quad (37)$$

The characteristics of the material are set to $\rho_{mat} = 2796 \text{ kg/m}^3$, $\sigma_{lim} = 372 \text{ MPa}$.

All of the analyses take less than 10 seconds altogether with the Intel Core 2 Quad processor.

2.3 Validation

To confirm the validity of aerodynamic force evaluation methods described so far, results of the present methods and CFD are compared.

2.3.1 Comparison with CFD in terms of pressure force

The present methods and CFD analyzed the same wing model to confirm the validity of the present methods in terms of pressure force.

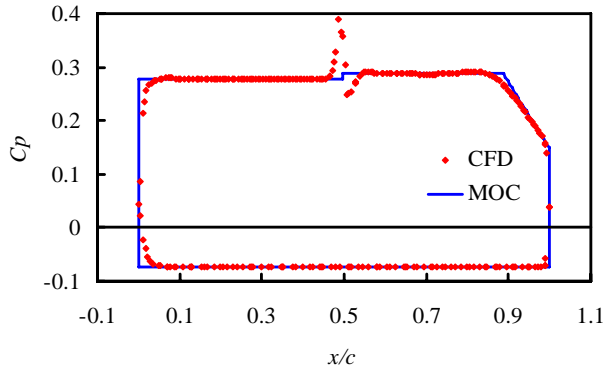
The wing model is shown in Fig. 6. The Mach number is set to 1.7. For CFD analysis, a flow solver named Tohoku University Aerodynamic Simulation code (TAS code) [13-18] using three-dimensional unstructured grid is employed. The three-dimensional Euler equations are solved by a finite-volume cell-vertex scheme. The lower/upper symmetric Gauss-Seidel (LU-SGS) implicit method for an unstructured grid is used for the time integration.



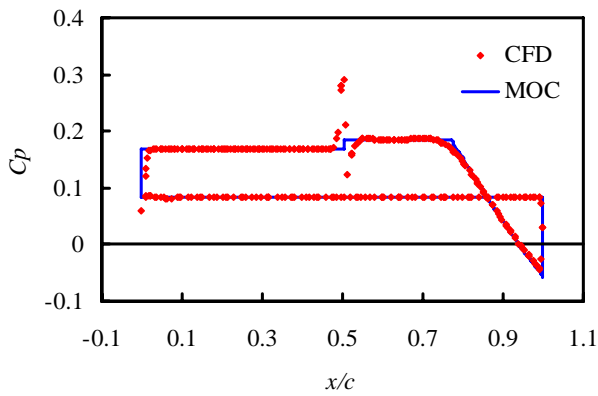
Fig. 6 Orthographic views of wing model used for validation

Figures 7 show the cross-sectional pressure coefficient distribution at 60% half span station. MOC indicates the result obtained from the present methods. Great agreement is confirmed between the results from the present method and

CFD except the region around the inward vertex located near $x/c=0.5$. The reason of the difference is that a shock wave has thickness of a couple of grid points in CFD resulting in gradual pressure rise around the vertex.



(a) Upper wing



(b) Lower wing

Fig. 7 Chordwise pressure coefficient distributions at 60% halfspanwise section

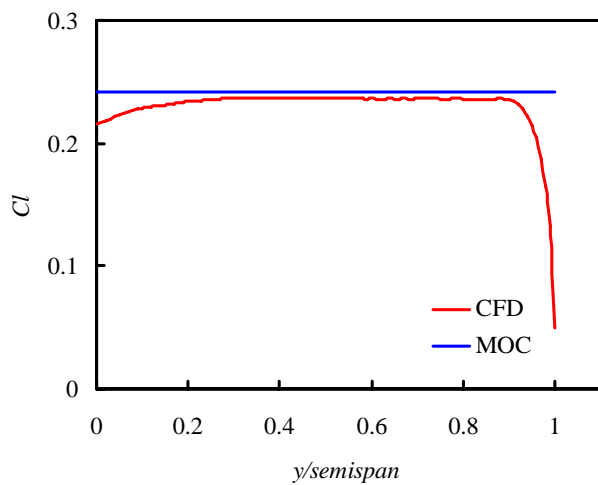


Fig. 8 Spanwise cross sectional pressure lift coefficient

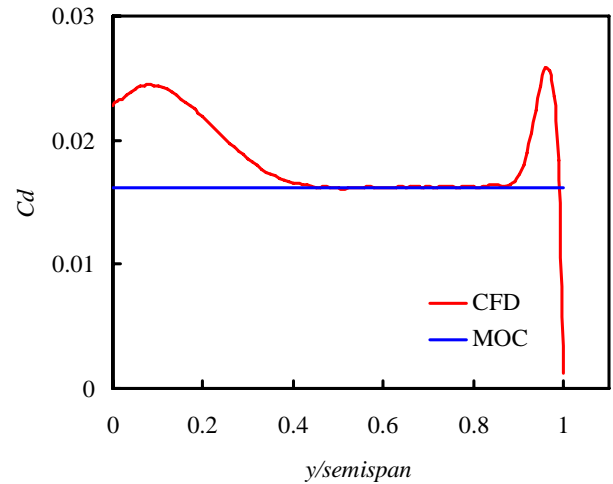


Fig. 9 Spanwise cross sectional pressure drag coefficient

Figures 8 and 9 show spanwise airfoil pressure lift and drag coefficients. It is confirmed that unideal regions exist near the wing tip and root, but good agreement between these two methods is achieved outside of the unideal regions.

As a conclusion, it is confirmed that the present methods can evaluate pressure force accurately in the ideal region but cannot evaluate pressure force in the unideal region. Hence, to conduct optimization using the present methods, it is necessary to assume that aerodynamic performance of the unideal region is independent of airfoil and to keep the planar shape of a wing unchanged to keep the size of the unideal region constant.

2.3.3 Comparison with CFD in terms of friction force

Friction force calculated by reference enthalpy method is compared with a result from CFD given in Ref. [4].

A wing model is constructed by straight lines and is symmetrical about a center line. Each wing has the thickness of 5%. For CFD analysis, Navier-Stokes equations were solved by TAS code. The Reynolds number based on the chord length of one wing is set to 3×10^7 . The Mach number is 1.7.

The results are shown in Table 1. Difference between the present method and CFD is about 10%. Considering the simplicity of the present method, those two methods agree fairly accurately.

Table 1 Drag coefficients of CFD and the present method

	CFD	Present	Error [%]
C_{dp}	0.0016	0.00177	+10.6
C_{df}	0.0087	0.00767	-11.8
C_d	0.0104	0.00944	-9.2

3 Optimization of Supersonic Biplane

3.1 Optimization Method

An optimizer called Adaptive Range Multi-Objective Genetic Algorithm (ARMOGA) [19] was employed for optimizations. ARMOGA uses Genetic Algorithm as an optimization algorithm. ARMOGA has the option to use adaptive range function, but it was not used. The number of individual members was 128. The initial population members were generated randomly across the whole design space. Fonseca and Fleming's Pareto ranking method was employed and fitness was computed based on average fitness. Stochastic Universal Selection (SUS) was employed as a selection method. The blended crossover was employed as a crossover method. The revised polynomial mutation was employed as a mutation method.

3.2 Single Objective Optimization of Supersonic Biplane

A single objective optimization to minimize pressure drag coefficient of a biplane with the same planar shape as the inversely designed wing [6] was conducted.

Design variables are the ratio of wing span to wing gap, dihedral angle of the lower wing, and variables shown in Fig. 2. The number of design variables is 15.

The result shown in Table 2 indicates that the present method found the design that has the pressure drag coefficient 11.0% lower than the ideal region of the design obtained by the inverse design method under almost the same condition of pressure lift coefficient. The inverse design method has a limitation of how to define the pressure distribution. The present aerodynamic performance evaluation method coupled with GA overcame the limitation and yields the better performance wing.

Table 2 Characteristics of supersonic biplanes obtained by the inverse design method and the optimization coupled with the present methods

	C_{Dp}	C_{Lp}	AR	t/c
Inverse design	0.00416	0.1138	5.120	0.1
Optimization	0.00370	0.1134	5.152	0.1014
Difference [%]	-11.0	-0.3	0.6	1.4

3.3 Multidisciplinary Optimization of Supersonic Biplane

3.3.1 Problem Definition

To conduct optimization, design variables, constraints, and objective functions need to be defined.

The taper ratio is fixed to 0.25. The previous studies [6,7] showed that tapered wings have good aerodynamic performance and, although it depends on the sweep angle, the taper ratio of around 0.25 yields the highest aerodynamic performance. The total wing area is set to greater than 230m², and the aspect ratio of each wing is set to greater than 6 to meet landing and climb requirements as described in Ref. 3. The sweep angle of lower wing leading edge is set to 11.3 degrees to make mid-chord sweep angle zero degree. The previous study shows that wings with mid-chord sweep angle of zero have a good aerodynamic performance [7].

The design variables are the same as the single objective optimization. The objective functions are drag and wing weight, both of which should be minimized.

The flight conditions were set as follows: the cruising weight is 50 metric tons, the cruising altitude is 55,000 ft, and the cruising Mach number is 1.7.

3.3.2 Results and Discussions

After evolving the population for 120 generations, the changes in objective functions became small. It indicates that the optimization has converged, so it was terminated at 120 generations. Figure 10 shows the drag and wing weight of the non-dominated solutions. Trade-off relationship between drag and wing weight is clearly observed. Consider the solution marked as A. If either drag or wing weight is reduced further, the other variable increases considerably. Hence, solution A is the most

likely candidate to be employed. The geometry of solution A is shown in Fig. 11.

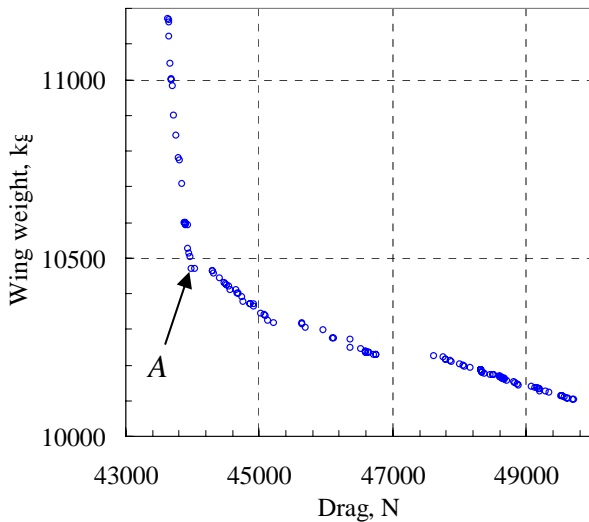


Fig. 10 Drag and wing weight of non-dominated solutions

Table 3 shows a comparison of the characteristics of the minimum drag design, a design A in Fig. 10, and the minimum wing weight design. The aerodynamic performance of the design A is worse than the inversely designed wing shown in Table 2. As shown in the section 3.2, the present tool has a potential to obtain higher aerodynamic performance wing, but it yielded lower aerodynamic wing because it considered not only pressure force but also friction force and weight.

Tendencies of the non-dominated solutions are as follows. First, thinner wings increase wing weight but decrease drag. Second, larger dihedral angles make the drag lower but make wing weight heavier. Thus, those parameters establish the trade-off relationship between drag and wing weight of the supersonic biplane.

For typical aircrafts, the weight of the wing is roughly 15% of the maximum takeoff weight [20]. Although it depends on how much fuel is consumed during takeoff and climb, the weight of the biplane is approximately 20% of the maximum takeoff weight. Hence, the biplane is relatively heavy, so it can be regarded as a drawback.

The lift to drag ratio is around 10. It is similar to that of delta or arrow wings that are usually used for supersonic aircrafts.

The wing fuel weight was evaluated by assuming that the wing can carry fuel of 85% of

the wing box's volume [20]. The biplane can store fuel that weighs over 20% of the cruising weight.

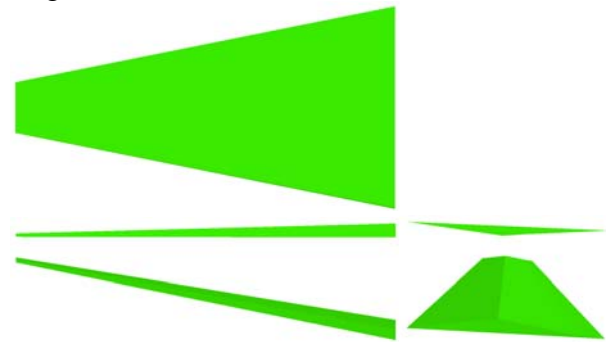


Fig. 11 Orthographic views of solution A

Table 3 Characteristics of solutions obtained from the multidisciplinary optimization

	Min. drag	A	Min. weight
Lift, N	489,142	489,166	489,176
Drag, N	43,637	43,995	49,712
C_{Lp}	0.2158	0.2289	0.2293
C_{Lj}	-0.0004	-0.0004	-0.0004
C_L	0.2154	0.2285	0.2289
C_{Dp}	0.0111	0.0124	0.0152
C_{Df}	0.0081	0.0081	0.0081
C_D	0.0192	0.0205	0.0233
$(L/D)_p$	19.44	18.43	15.12
L/D	11.21	11.12	9.84
Total wing weight, kg	11,169	10,471	10,101
Wing weight, lower wing, kg	4,912	4,709	4,661
Wing weight, upper wing, kg	6,257	5,762	5,441
Aspect ratio, lower wing	6.31	6.13	6.01
Aspect ratio, upper wing	6.02	6.03	6.02
Total wing area, m ²	244	230	230
Wing area, lower wing, m ²	119	114	115
Wing area, upper wing, m ²	125	116	115
Span length, m	27.4	26.5	26.3
Sweep angle, leading edge, lower wing, deg.	11.3	11.3	11.3
Sweep angle, leading edge, upper wing, deg.	11.2	11.2	11.1
Dihedral angle, leading edge, lower wing, deg.	11.5	10.3	7.5
Dihedral angle, leading edge, upper wing, deg.	-0.2	-1.5	-5.5
α , lower wing, deg.	2.94035	3.1042	3.07947
α , upper wing, deg.	2.52559	2.50337	2.45174
t/c , lower wing, %	7.07	7.30	7.63
t/c , upper wing, %	4.80	4.87	5.29
Total usable wing fuel, kg	12,473	11,853	13,809
Usable wing fuel, lower wing, kg	8,565	8,371	9,767
Usable wing fuel, upper wing, kg	6,109	5,573	6,479

4 Conclusions

The tool to evaluate the performance of a supersonic biplane has been developed using the modified oblique shock wave equations, the modified Method of Characteristics, and the reference enthalpy method. It has been confirmed that aerodynamic forces can be evaluated with less than the error of 12% in the ideal region of the test case compared to CFD at significantly low computational costs.

Using the tool thus developed, the multidisciplinary optimization was conducted to

design a three-dimensional supersonic biplane. The high performance wings were obtained and the major factors governing the trade-off relationship between drag and wing weight were found out. Small thickness-to-chord ratio and larger dihedral angle decrease drag but increase wing weight. The characteristics of a supersonic biplane were also shown. The aerodynamic performance is similar to that of a delta or an arrow wing. Supersonic biplanes are relatively heavy, and can store fuel that weighs over 20% of the cruising weight.

Acknowledgments

This study was supported by IFS Graduate Student Overseas Presentation Award.

References

- [1] Busemann A. Auftrieb des doppeldeckers bei überschallgeschwindigkeit. *Convegno di Scienze Fisiche, Matematiche e Naturali, Le Alte Velocità in Aviazione*, pp 356-360, 1936. (in German)
- [2] Lomax H. The wave drag of arbitrary configurations in linearized flow as determined by areas and forces in oblique planes. NACA RM A55A18, 1955.
- [3] Utsumi Y and Obayashi S. Design of supersonic biplane aircraft concerning sonic boom minimization. *Proc 28th AIAA Applied Aerodynamics Conference*, AIAA-2010-4962, 2010.
- [4] Kusunose K, et al. *Aerodynamic design of supersonic biplane: cutting edge and related topics*. The 21st century COE program, International COE of flow dynamics, Lecture series, Vol. 5, Tohoku University Press, Sendai, Japan, 2007.
- [5] Maruyama D, et al. Aerodynamic design of three-dimensional low wave-drag biplanes using inverse problem method. *Proc AIAA Aerospace Sciences Meeting and Exhibit*, AIAA-2008-289, 2008.
- [6] Maruyama D. Aerodynamic design of three-dimensional biplane wings for low wave-drag supersonic flight. *Proc International Congress of the Aeronautical Sciences*, 2008.
- [7] Yonezawa M and Obayashi S. Aerodynamic performance of the three-dimensional lifting supersonic biplane. *Journal of Aircraft*, Vol. 47, No. 3, pp 983-991, 2010.
- [8] Licher R M. Optimum two-dimensional multiplanes in supersonic flow. Report No. SM-18688, Douglas Aircraft Co., 1955.
- [9] Liepmann H W and Roshko A. *Elements of Gasdynamics*. Dover Publications, 2002.
- [10] Meador W E and Smart M K. Reference enthalpy method developed from solutions of the boundary-layer equations. *AIAA Journal*, Vol. 43, No. 1, pp 135-139, 2005.
- [11] Leoviriyakit K. Wing planform optimization via an adjoint method. Ph.D Diss., Stanford Univ., 2005.
- [12] Noguchi R, Maruyama D, Matsushima K and Nakahashi K. Study of the aerodynamic center and aerodynamic characteristics of supersonic biplanes in a wide Mach number range. *Proc 22th CFD Symposium*, 2008. (in Japanese)
- [13] Ito Y and Nakahashi K. Direct surface triangulation using stereolithography data. *AIAA Journal*, Vol. 40, No. 3, pp 490-496, March 2002.
- [14] Ito Y and Nakahashi K. Surface triangulation for polygonal models based on CAD data. *International Journal for Numerical Methods in Fluids*, Vol. 39, Issue 1, pp 75-96, May 2002.
- [15] Sharov D and Nakahashi K. A boundary recovery algorithm for delaunay tetrahedral meshing. *Proc 5th International Conference on Numerical Grid Generation in Computational Field Simulations*, pp 229-238, 1996.
- [16] Nakahashi K, Ito Y and Togashi F. Some challenge of realistic flow simulations by unstructured grid CFD. *International Journal for Numerical Methods in Fluids*, Vol. 43, pp 769-783, 2003.
- [17] Obayashi S and Guruswamy G P. Convergence acceleration of a Navier-Stokes solver for efficient static aeroelastic computations. *AIAA Journal*, Vol. 33, No. 6, pp 1134-1141, 1995.
- [18] Sharov D and Nakahashi K. Reordering of hybrid unstructured grids for lower-upper symmetric Gauss-Seidel computations. *AIAA Journal*, Vol. 36, No. 3, pp 484-486, 1998.
- [19] Sasaki D and Obayashi S. Efficient search for trade-offs by adaptive range multi-objective genetic algorithms. *Journal of Aerospace Computing, Information, and Communication*, Vol. 2, pp 44-64, 2005.
- [20] Raymer D P. *Aircraft design: A conceptual approach*. Forth ed., AIAA Education Series, AIAA, 2006.

Copyright Statement

The authors confirm that they, and/or their company or organization, hold copyright on all of the original material included in this paper. The authors also confirm that they have obtained permission, from the copyright holder of any third party material included in this paper, to publish it as part of their paper. The authors confirm that they give permission, or have obtained permission from the copyright holder of this paper, for the publication and distribution of this paper as part of the ICAS2010 proceedings or as individual off-prints from the proceedings.